Overview of Electrons and Orbitals in a Nearly One-Dimensional Co^{3+}/Co^{4+} System

Matthieu Kauffmann,[†] Olivier Mentré,*[,†] Alexandre Legris,[‡] Sylvie Hébert,[§] Alain Pautrat,[§] and Pascal Roussel[†]

UCCS, Equipe Chimie du Solide, CNRS UMR 8181, ENSC Lille−UST Lille, BP 90108, 59652 Villeneuve d'Ascq cedex, France, Laboratoire de Métallurgie Physique et Génie des Matériaux (LMPGM), CNRS UMR 8517, ENSC Lille−UST Lille, 59655 Villeneuve d'Ascq cedex, France, and Laboratoire CRISMAT, UMR 6508 CNRS-ENSICAEN, 6 boulevard Maréchal Juin, 14050 Caen cedex, France

Received September 19, 2007. Revised Manuscript Received December 3, 2007

$Ba_6Co_6ClO_{15.5}$ has been analyzed from the point of view of local electric/magnetic interactions and orbital overlapping, step by step following the different subunits of the crystal structure. Our investigation is based on structural data (X-ray and neutron diffraction, hereafter XRD and ND), experimental magnetic/electric/transport measurements, magnetic structure, and density functional theory (DFT) calculations. Its crystal structure is related to the 12H-$BaCoO_{3-\delta}$ form and contains corner sharing pairs of Co^{4+} tetrahedra, with strong antiferromagnetic (AF) exchanges (estimation of $J \sim 0.07$ eV). In the title compound, Co^{4+} are assigned to "intermediate spin" IS with electronic configuration $e_g^3t_{2g}^2$, $S = {}^3/_2$. This rather rare configuration for a d^5 cation is explained from the splitting of the t_{2g} manifold because of an important off-centering of the shared corner. The dimers are connected to linear $Co^{3+}{}_4O_{15}$ subunits, and both tetrahedral−tetrahedral and tetrahedral−octahedral magnetic junctions have been explored by the analysis of the correlation and delocalization Co−O−Co superexchanges, in good agreement with the experimental results. The tetrameric units have been assigned to an ordered mixture of HS and LS Co^{3+} while below T_N, and the localized magnetic moments vanished because of electron transfer toward covalent oxygen ligands and by direct exchanges in the intermediate Co−Co region. Then, the electrons are confined inside these units, which act as strong ferromagnetic connectors between the terminal Co^{4+} tetrahedra. The overview of the transport properties (conductivity, thermoelectric power, and positive magnetoresistance) are in favor of a variable range hoping (VRH) regime below T_N produced by an Anderson-like localization, in which tetrahedral Co^{4+} play the role of disordered centers with respect to a 1D system.

1. Introduction

$BaCoO_3$ is a structurally one-dimensional 2H hexagonal perovskite, with many of its derivatives mainly conserving this reminiscent characteristic because of the strong preference of hexacoordinated cobalt for face-sharing assemblies. In the last few decades, much attention has been paid to the remarkable properties induced by their low-dimensional magnetic and electric characteristics. For instance, the series of $A_{n+2}Co_{n+1}O_{3n+3}$ (A = Ca, Ba, etc.) cobaltites compounds display 1D columns of face-sharing CoO_6 octahedra and prisms in an ordered manner,[1,2] and the term with $n = 1$, $Ca_3Co_2O_6$, has been investigated, leading to the evidence of low spin (LS) and high spin (HS) alternation responsible for giant orbital moment and for the resulting intra- and interchain ferromagnetic (F) coupling.[3] In the parent compound $BaCoO_3$ with LS Co^{4+} ($S = {}^1/_2$), the ground-state origin is not fully understood but the intrachains interactions are preferentially ferromagnetic along *c* and a competition between F and AF interchain interactions would produce a weak ferromagnet at low temperature, i.e., $M^{5T} = 0.15$ μB/Co.[4,5] However, the possibility of superparamagnetism between noninteracting ferromagnetic clusters embedded in a nonferromagnetic matrix has been recently argued.[6] In this latter, Anderson localization is argued to explain the poor conductivity as well as in the n-doped $Ba_{1-x}La_xCoO_3$.[7] In the 2H-$BaCoO_3$, the creation of ordered oxygen vacancies leads to two polymorphs, the 5H and 12H forms, which conserve linear fragments of face-sharing octahedra (trimeric and tetrameric units, respectively) with terminal tetrahedra breaking the 1D character. Both compounds order ferromagnetically, and the latter has also been shown to behave as a low-dimensional semiconductor with an ordered local-

* To whom correspondence should be addressed. E-mail: olivier.mentre@ensc-lille.fr.
† UCCS, Equipe Chimie du Solide.
‡ Laboratoire de Métallurgie Physique et Génie des Matériaux (LMPGM).
§ Laboratoire CRISMAT.

(1) Darriet, J.; Elcoro, L.; El Abed, A.; Gaudin, E.; Perez-Mato, J. M. *Chem. Mater.* **2002**, *14*, 3349.
(2) Boulahya, K.; Parras, M.; Gonzalez-Calbet, J. M.; Vegas, A. *J. Solid State Chem.* **2000**, *151*, 77.
(3) Wu, H.; Haverkort, M. W.; Hu, Z.; Khomskii, D. I.; Tjeng, L. H. *Phys. Rev. Lett.* **2005**, *95*, 186401.
(4) Pardo, V.; Blaha, P.; Iglesias, M.; Schwarz, K.; Baldomir, D.; Arias, J. E. *Phys. Rev. B: Condens. Matter Mater. Phys.* **2004**, *70*, 144422.
(5) Yamaura, K.; Cava, R. J. *Solid State Commun.* **2000**, *115*, 301.
(6) Pardo, V.; Rivas, J.; Baldomir, D.; Iglesias, M.; Blaha, P.; Schwartz, K.; Arias, J. E. *Phys. Rev. B: Condens. Matter Mater. Phys.* **2004**, *70*, 212404.
(7) Yamaura, K.; Cava, R. J. *Solid State Commun.* **2000**, *115*, 301.

10.1021/cm702678v CCC: $40.75
Published on Web 01/23/2008

ization state of the carriers.[8] In the frame of the prospecting for new oxides and oxyhalides leading, for instance, to the recent $Ba_2Co_9O_{14}$ phase,[9,10] a number of strongly related materials have been isolated and characterized, e.g., $Ba_5Co_5XO_{13}$ and $Ba_6Co_6XO_{15.5}$ (X = F, Cl),[11–13] $Ba_6Co_5BrO_{14}$ and $Ba_7Co_6BrO_{16.5}$,[14] and $Ba_2Co_4XO_7$ (X = Cl, Br).[15] Most of these compounds display either tri- or tetrameric units, reminiscent of $BaCoO_{3-\delta}$, which are connected or not, depending upon the halide-containing layer. Among them, $Ba_6Co_6ClO_{15.5}$ has been the subject of particular investigations[16] that revealed AF magnetic ordering ground state, on the opposite to the parent $BaCoO_{3-\delta}$. This work is devoted to the accurate investigation of the electronic- and magnetic-involved mechanisms, using a set of experimental and theoretical data. The verification of magnetic exchanges in several subunits of the structure has been particularly investigated by means of the orbital overlapping and the Kanamori−Goodenough−Anderson rules, as well as the transport properties against those of the parent compounds.

2. Experimental Section

Polycrystalline powder of $Ba_6Co_6ClO_{15.5}$ was synthesized following the route described in a previous paper.[12] Neutron powder diffraction data were collected at room temperature, 140, 130, 120, 110, and 3 K on the high-resolution powder diffractometer D2B at the neutron facility Institut Laue-Langevin (ILL Grenoble, France) equipped with a cryostat. The step scan covered a 2θ range of 4.00–160.00° with a step length of 0.05°. For nuclear structure assignment at room temperature, a monochromatic wavelength of 1.594 Å was used, while measurements at 3K were performed both with the wavelength at 1.594 Å to refine the nuclear structure and at 2.398 Å to refine the magnetic structure. The diffraction data were refined by the Rietveld method using the FULLPROF software.[17] Scattering lengths and form factors for Ba, Co, Cl, and O were taken from the library of the program. Each structural model was refined to convergence, and the best result was chosen on the basis of agreement factors.

The magnetic susceptibility and the electric resistivity have both been measured using an Oxford Maglab EXA 9T system. The susceptibility measurement was performed by the DC extraction method under an applied field of 1.0 T from room temperature down to 3 K. The susceptibility has been corrected from the sample and the sample holder diamagnetism. The electric resistance has been measured using the four probe method on a bar shaped with an uniaxal press and then sintered at 900 °C in a tubular furnace. Colloidal silver paint was deposited on the sample, and 50 μm thick gold wires were attached with silver-saturated epoxy. The DC current imposed through the two extremities was 100 nA. The resistivity was deduced by the estimation of the *l*/*s* factor (=10 cm^{-1}). The thermopower has been measured using a standard steady-state technique, in a puck especially designed and inserted in a PPMS (Quantum Design) system. The magnetoresitance measurements were performed in a 14 T PPMS (Quantum Design) system. The magnetoresistance data were taken at a fixed temperature when cooling the sample.

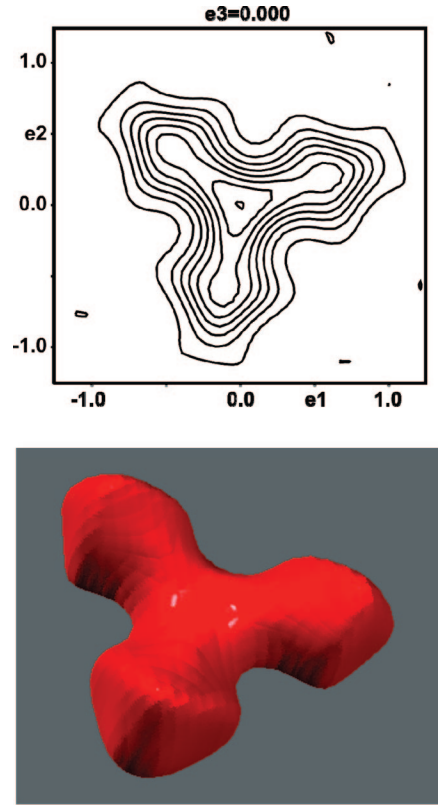

Figure 1. Two- and three-dimensional representations of the electronic density calculated by MEM for the O(4) atom.

3. Result and Discussion

3.1. Atomic Structure. The neutron powder diffraction pattern obtained at room temperature was used for the accurate refinement of oxygen occupancies. The difference pattern as well as agreement factors (R_{wp}, 0.092; R_p, 0.096; R_F, 0.019; R_{Bragg}, 0.028; and R_{exp}, 0.160) show the quality of the refined model. It results in an occupancy of 0.94(1) for O(1) (site 6n) and 0.96(1) for O(3) (site 3k) [while O(2) refined to full occupancy], leading to the formula $Ba_6Co_6ClO_{15.52(1)}$, thus confirming the redox chemical analysis reported in our previous paper.[12] Another point was tackled in the single crystal structure determination: a disorder was detected around the oxygen atom of the [BaOCl] layer. The O(4) atom was found to occupy the vertex of a little triangle around the 3-fold axis. For a better accuracy on the electron density distribution on this disordered site, a maximum entropy method (MEM) algorithm was used to plot maps. It is clearly seen that the O(4) is distributed over the 3-fold axis (Figure 1). This splitting of the vertex of the tetrahedron could be responsible for the

(8) Boulahya, K.; Parras, M.; Gonzalez-Calbet, J. M.; Amador, U.; Martinez, J. L.; Tissen, V.; Fernandez-Diaz, M. T. *Phys. Rev. B: Condens. Matter Mater. Phys.* **2005**, *71*, 144402.
(9) Sun, J.; Yang, M.; Li, G.; Yang, T.; Liao, F.; Wang, Y.; Xiong, M.; Lin, J. *Inorg. Chem.* **2006**, *45*, 9151.
(10) Ehora, G.; Daviero-Minaud, S.; Colmont, M.; André, G.; Mentré, O. *Chem. Mater.* **2007**, *19*, 2180.
(11) Yamaura, K.; Young, D. P.; Siegrist, T.; Besnard, C.; Svensson, C.; Liu, Y.; Cava, R. J. *J. Solid State Chem.* **2001**, *158*, 175.
(12) Tancret, N.; Roussel, P.; Abraham, F. *J. Solid State Chem.* **2005**, *178*, 3066.
(13) Ehora, G.; Renard, C.; Daviero-Minaud, S.; Mentré, O. *Chem. Mater.* **2007**, *19*, 2924.
(14) Kauffmann, M.; Roussel, P. *Acta Crystallogr., Sect. B: Struct. Sci.* **2007**, *63*, 589.
(15) Kauffmann, M.; Tancret, N.; Abraham, F.; Roussel, P. *Solid State Sci.* **2007**, *9*, 885.
(16) Kauffmann, M.; Mentre, O.; Legris, A.; Tancret, N.; Abraham, F.; Roussel, P. *Chem. Phys. Lett.* **2006**, *432*, 88.
(17) Rodriguez-Carvajal, J. *Physica B* **1993**, *192*, 55.

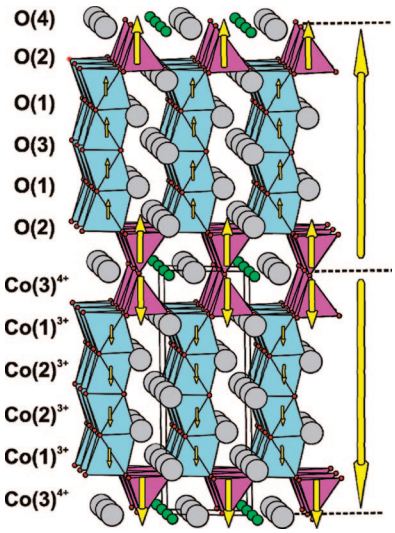

Figure 2. Layered structure of $Ba_6Co_6ClO_{15.5}$. Oxygen lacunar sites are denoted with a L. The arrows indicate the spin orientation of the most stable magnetic structures as determined from neutron diffraction (ND) and DFT calculations. Values of the fitted moments are given on the right for both techniques.

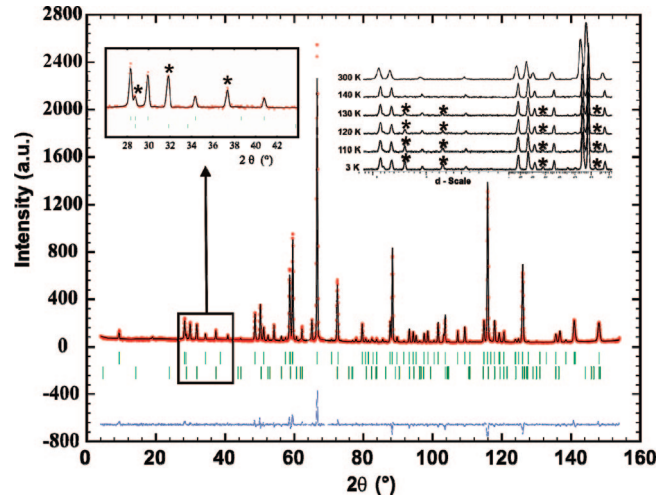

Figure 3. Observed and calculated neutron diffraction patterns and their difference for $Ba_6Co_6ClO_{15.5}$ at 4 K with the neutron beam of wavelength at 2.398 Å. The inset shows the neutron patterns as a function of the temperature. The stars denote the magnetic reflections.

stabilization of a particular spin intermediate state for the tetrahedral cobalt. Finally, a combined refinement with neutron powder (λ = 1.594 Å), X-ray powder ($\lambda K_{\alpha 1\text{-Cu}}$ = 1.54056 Å), and X-ray single-crystal data ($\lambda K_{\alpha\text{-Mo}}$ = 0.71073 Å) was conducted using the beta version of JANA2006. Atomic coordinates, anisotropic displacement parameters, and experimental details are available in the Supporting Information. A view of the structure, in projection along [010] is given in Figure 2. It shows the localization of the oxygen lacunar [BaO_3] layers, which contribute to the octahedral environment of central cobalt Co(2) of the tetrameric subunits. The resulting average cobalt oxidation state is +3.33, a value which deserves special comments:

(i) It has been explained by a valence ordered site model with Co^{4+} in tetrahedral [Co(3) site] and Co^{3+} in octahedral ones [Co(1) and Co(2)].[16] The Co(3)−O bond distances [3 × 1.843(3) and 1 × 1.865(5) Å at room temperature] suggests tetravalent Co as already discussed for the analogue oxyfluorides.[13] Furthermore, the shorter average Co(2)−O bond length [3 × 1.885(2) and 1 × 1.897(2) Å] against the Co(1)−O bond distance [3 × 1.923(3) and 1 × 1.926(2) Å] is also consistent with LS/HS segregation in these sites. Of course, one should consider the possibility of partial hole-doping in the tetrameric units because of extra oxygen vacancies. It yields the emptying of the most antibonding states and could participate to the short Co−Co distances [2.4782(9) Å from single-crystal data].

(ii) Another attractive model, according to the refined magnetic structure to be presented, involves HS Co^{3+} in the tetrahedral sites and mixed valence LS $Co^{3.5+}$ in the linear subunits, on the basis of the magnetic structure refinement. Once more, the two holes created by the mixed valence would introduce some extra Co−Co bonding along *c*. However, the hypothesis of tetrahedral Co^{3+} is rather unlikely in this compound, taking into account the strong preference of tetravalent cobalt in this environment, e.g., consensus about tetrahedral Co^{4+} in $BaCoO_{3-\delta}$, tetrahedral Co^{4+} in Ba_2CoO_4, etc. Furthermore, the corresponding effective moment would be far from the observed value (see the section dedicated to magnetism). This hypothesis has not been validated.

3.2. Magnetic Structure. Neutron powder diffraction data for $Ba_6Co_6ClO_{15.5}$ were collected from room temperature to 4 K using the D2B diffractometer. The inset in Figure 3 presents the neutron patterns as a function of the temperature. As briefly reported in ref 16, the pattern below T_N = 135 K revealed the occurrence of long-range antiferromagnetic ordering. The magnetic satellites are indexed using the propagation vector k = [0, 0, $^1/_2$]. In the nuclear unit cell, the Co atoms are found on the 2h and 2i sites, leading to six magnetic positions by primitive cell. For these sites, according to k = [0, 0, $^1/_2$], the decomposition of the magnetic representation is

$$\Gamma = 0\Gamma_1^{(1)} + 1\Gamma_2^{(1)} + 1\Gamma_3^{(1)} + 0\Gamma_4^{(1)} + 1\Gamma_5^{(2)} + 1\Gamma_6^{(2)}$$

The absence of any 00*l* magnetic satellite involves magnetic moments collinear to the *c* axis. Therefore, only one-dimensional representations, Γ_2 and Γ_3, are compatible with our compound because they correspond to atomic moments aligned along *c*. Our refinement validates the Γ_2 model with ferromagnetic cobalt atoms within blocks. Blocks are antiferromagnetically juxtaposed through the spin reversal induced by the propagation vector. The nuclear structure (atomic position and anisotropic displacement parameters) has been refined at λ = 1.594 Å. Then, the positions of magnetic atoms have been fixed, while the magnetic moments of Co were refined using data collected at λ = 2.398 Å. Except contraction of the cell parameters because of thermal effect, no structural change was observed at 3 K [a = 5.656(1) Å and c = 14.487(1) Å] compared to RT [a = 5.670(1) Å and c = 14.516(1) Å]. The refined moments at 4 K are $m_{Co(3)} = 2.82(5)\ \mu_B$, while $m_{Co(1)}$ and $m_{Co(2)}$ are about 0. The later were set to 0 in the last cycles without significant change of the reliability factors. Figure 3 shows the observed and calculated neutron diffraction patterns at 4 K, λ = 2.398 Å. The final reliability factors are R_{wp}, 0.107; R_p, 0.108; R_F, 0.025; R_{Bragg}, 0.040; R_{exp}, 0.231; and $R_{magnetic}$, 0.140 (λ, 1.594

Å; T, 4 K) and R_{wp}, 0.154; R_p, 0.177; R_F, 0.043; R_{Bragg}, 0.083; R_{exp}, 0.221; and $R_{magnetic}$, 0.093 (λ, 2.398 Å; T, 4 K). A view of the magnetic structure, in projection along [010], is given in Figure 2.

3.3. DFT Calculations. To assess basic properties of the compound and to obtain information concerning octahedral cobalt atoms, electronic structure calculations have been performed. The calculations were done using the *ab initio* total-energy calculation package Vienna *ab initio* simulation program (VASP)[18–20] a code based on the DFT that determines the total energy of a periodic system without any experimental input but the chemical nature of the atoms. The results presented here were obtained allowing spin polarization using the generalized gradient approximation (GGA) for the exchange-correlation potential derived by Perdew and Wang.[21] The calculations were performed using ultrasoft pseudopotentials[22,23] to describe ionic cores, and the parameters employed are those described in detail in ref 16.

The calculations yield an antiferromagnetic ground state obtained by the alignment of two simple cells along the c axis. Within each simple cell (i.e., nuclear ones), all Co have a ferromagnetic ordering, the magnitude of the spin depending upon the position along the Co chains in good agreement with the experimental result. Tetrahedral Co(3) ions carry out 2.3 μ_B [2.82(5) μ_B by ND], and octahedral Co(1) and Co(2) carry out 0.6 and 0.5 μ_B, respectively (0−0.5 μ_B by ND). Finally, the O(2) (at the tetrahedral/octahedral junction) is associated with a 0.3 μ_B moment. Concerning the various possible alignments between the spins, the following results have been found:

(i) Although the magnetic moments of Co(1) are relatively low, the Co(3)−Co(1) magnetic interaction has a strong ferromagnetic character and no stable antiferromagnetic configuration between Co(3) and Co(1) was found.

(ii) Flipping the magnetic moments into a ferromagnetic structure costs a total energy of 0.23 eV per simple unit cell above the ground state. This energy increase allows us to estimate the antiferromagnetic exchange interaction per Co(3)−Co(3) contact to be close to 0.115 eV.

(iii) The lowest energy magnetic structures have Co(2)−Co(2) (∼0.10 eV) and Co(1)−Co(2) (∼0.04 eV) ferromagnetic ordering, although highest energy metastable structures with antiferromagnetic couplings can be obtained.

From a structural point of view, after the relaxation of the structure at 0 K, the calculated Co(1)−Co(2) and Co(2)−Co(2) distances are 2.54 and 2.47 Å, respectively, in good agreement with our structural data. The $Co(1)O_6$ and $Co(2)O_6$ octahedra are also slightly shortened because the mean Co(1)−O distance is close to 1.94 Å, while the corresponding value for Co(2)−O is 1.90 Å. At least no important atomic displacement occurs within the tetrameric subunits from room temperature to 0 K.

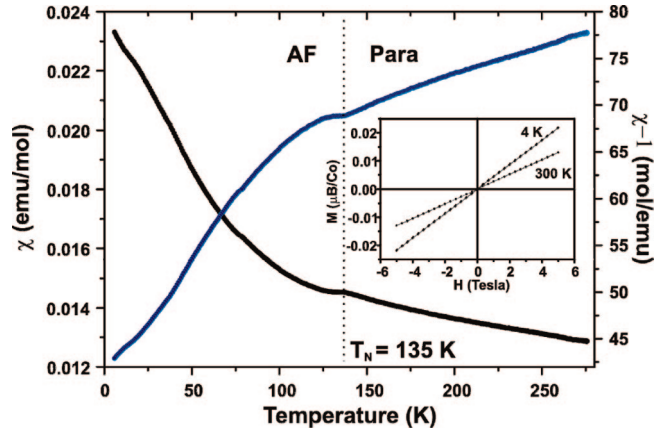

Figure 4. Dependence on the temperature of the inverse of magnetic susceptibility for $Ba_6Co_6ClO_{15.5}$ from room temperature to 3 K. The inset shows the magnetization (normalized per cobalt) versus applied magnetic field at 300 and 4 K.

3.4. Magnetic Behavior. In our previous work dealing with the AF ordering in $Ba_6Co_6ClO_{15.5}$,[16] the magnetic/electric characterization has been skimmed over; notably, the comparison between intrinsic properties of the title compounds and related $BaCoO_{3-\delta}$ materials appears of the highest interest. Figure 4 presents the plot of χ and its inverse against T, under an applied field of 1.0 T. No noticeable difference was found between the ZFC and FC curves. The increasing of χ below T_N is probably originated by the existence of large ferromagnetic domains isolated by the [BaOCl] layers. Then, crystal defects and surfaces should contain a part of uncompensated moment. In the high-temperature domain, it obeys a Curie–Weiss-like law with $\mu_{eff} = 10.84$ μ_B/fu, $\theta_{CW} = -942$ K, and $\chi_{VV} = 0.000\,79$ emu/mol, where χ_{VV} is the second-order Van-Vleck constant paramagnetism, expected to be important in our case. However, when the huge value of θ_{CW} complicated by the low dimensionality of the crystal structure is taken into account, the interpretation of these data is rather ambiguous. It may picture the superposition of several phenomena, including true paramagnetism and Pauli-like magnetism. Nevertheless, the negative θ_{CW} value is in agreement with the AF ordering appearing at medium temperature, $T_N = 135$ K, and the μ_{eff} value can be considered as significant in a first approach. The localized moments are confirmed by the semiconducting behavior detailed below. When the refined local magnetic moments of 2.82(5) μB for Co(3) are taken into account, confirmed by our DFT calculation [$m = 2.3$ μ_B/Co(3)], it was assigned to intermediate spin (IS) $S = {}^3/_2$ tetrahedral Co^{4+}. This selected rare configuration of d^5 cations is detailed in the next section. Thus, assuming Co^{4+} as IS, the nine possible distributions of spin states in the Co^{3+} tetramers are gathered in Table 1.

Considering the difference between the geometries of $Co(1)O_6$ and $Co(2)O_6$ octahedra [characterized by distances of 1.930(8) and 1.898(7) Å, respectively] and taking into account the difference of ionic radii for HS and LS Co^{3+},[12] the most reasonable model involves a distribution of LS in Co(2) and HS in Co(1). The discrepancy between calculated

(18) Kresse, G.; Hafner, J. *Phys. Rev. B: Condens. Matter Mater. Phys.* **1993**, *47*, R558.
(19) Kresse, G.; Furthmüller, J. *Phys. Rev. B: Condens. Matter Mater. Phys.* **1996**, *54*, 11169.
(20) Kresse, G.; Furthmüller, J. *Comput. Mater. Sci.* **1996**, *6*, 15.
(21) Perdew, J. P.; Wang, Y. *Phys. Rev. B: Condens. Matter Mater. Phys.* **1991**, *45*, 13244.
(22) Vanderbilt, D. *Phys. Rev. B: Condens. Matter Mater. Phys.* **1990**, *41*, R7892.
(23) Kresse, G.; Hafner, J. *J. Phys.: Condens. Matter* **1996**, *6*, 8245.

Table 1. Possible Distributions of Spin States in the Co^{3+} Tetramers, Considering IS $Co(3)^{4+}$ ($S = {}^3/_2$) and Calculated Effective Moments in a Spin-Only Approximation

spin distribution	μ_{eff} theoretical (μ_B/fu)	g_S	percent orbital contribution (%)
$Co(1)^{3+}$ LS−$Co(2)^{3+}$ LS	5.47	3.96	49
$Co(1)^{3+}$ LS−$Co(2)^{3+}$ IS	6.78	3.20	37
$Co(1)^{3+}$ IS−$Co(2)^{3+}$ LS	6.78	3.20	37
$Co(1)^{3+}$ IS−$Co(2)^{3+}$ IS	7.87	2.75	27
$Co(1)^{3+}$ LS−$Co(2)^{3+}$ HS	8.83	2.45	18
$Co(1)^{3+}$ HS−$Co(2)^{3+}$ LS	8.83	2.45	18
$Co(1)^{3+}$ IS−$Co(2)^{3+}$ HS	9.69	2.23	11
$Co(1)^{3+}$ HS−$Co(2)^{3+}$ IS	9.69	2.23	11
$Co(1)^{3+}$ HS−$Co(2)^{3+}$ HS	11.22	1.93	−3

(8.83 μ_B/fu) and observed μ_{eff} (10.84 μ_B/fu) are explained by the high Ising-like magnetic anisotropy of cobalt mainly because of the important orbital contribution.[24] In Table 1, the so-called orbital contribution denotes the discrepancy between the experimental and theoretical spin-only value of μ_{eff}. This difference is noticeable through the g_S calculation on the basis of μ_{eff} experimental $= g_S\sum_i n_i(S_i)(S_i + 1)$, with n_i being the stoichiometric coefficient of each independent cation per $Ba_6Co_6ClO_{15.5}$ formula unit. Note that the tetrahedral HS Co^{3+}−octahedral LS Co^{3+}/Co^{4+} model briefly exposed above leads to the rather low $\mu_{eff} = 7.34\ \mu$B/fu value in the spin-only approximation.

The magnetization plots at 4 and 300 K are shown in the inset of Figure 4. No residual magnetic contribution appears below T_N excluding spin-canting effects. According to its exaggeratedly high value for an oxide, θ_{CW} should be carefully manipulated. In the mean field approximation, it is defined by $\theta_{CW} = ((zS(S + 1))/3)(J/k)$, where $S = {}^3/_2$ for the IS Co^{4+}, J is the spin-exchange parameter within dimers, z is the number of nearest neighbor magnetic sites around a given Co^{4+} (i.e., 1 in our purpose), and k is the Boltzmann constant. In the present case, considering that the AF couplings of dimers is solely responsible for θ_{CW} and neglecting the contribution of the weaker ferromagnetic exchanges, it leads to $J = 0.07$ eV. This value is in correct agreement with the energy gain to reverse the magnetic structure into a ferromagnetic state calculated by DFT. In this calculation, two AF Co^{4+}-Co^{4+} contacts are broken and, consequently, the resulting value has to be divided by two, yielding $J_{DFT} = 0.23$ eV/2 $= 0.115$ eV. Whatever the reasons for the slight discrepancy between the experimental and calculated J are, the AF coupling still appears very strong.

3.5. Tetrahedral IS Co^{4+}. Our assignment of the IS state in the tetrahedral Co^{4+} mainly stems from the ND data and DFT calculations giving comparable moment of 2.8 and 2.3 μ_B for Co(3). As a matter of fact, neither LS Co^{4+} ($S = {}^1/_2$) nor HS Co^{4+} ($S = {}^5/_2$) match these results, nor the value of the effective moment, otherwise involving either a huge orbital contribution or a considerable dilution of the moment through Co−O covalence effects, for instance. It is well-known that the spin crossover arising in some transition-metal cations is the result of the competition between the values of the crystal field parameter (D_q), the intra-atomic exchange energy (J_H), and interelectronic Coulombic repulsion energies (U and U'). Then, a number of cobaltites $La_{1-x}Sr_xCoO_3$[25–27] exhibit various Co^{3+} and Co^{4+} spin states versus the temperature. To clarify this competition, Pouchard et al.[28] have performed theoretical calculations combining the internal electronic exchange, the crystal field, and the local symmetry for $3d^{4,5,6}$ transition-metal oxides. According to their results, the so-called IS d^5 cation in tetrahedral symmetry appears highly contestable, because only $S = {}^1/_2$ and ${}^5/_2$ spin states appear stable with varying the J_H/D_q ratio. However, the crystallographic refinement and the MEM analysis clearly evidenced the important off-centering of O(4) in the basal plane, 0.63 Å away from its ideal special position. It is noticeable that similar splitting also exists in the fluoride analogues, $Ba_6Co_6FO_{15.5}$ and $Ba_5Co_5FO_{13}$, and was attributed to a balancing displacement toward the underbonded in-plane Ba^{2+} cation.[13] Then, for these series of compounds, a probable scenario over the resulting orbital diagram is presented in Figure 5. In fact, the O(4) displacement is expected to split the t_{2g} manifold into a low lying doublet and a higher lying singlet, leading to the $e_g{}^3t_{2g}{}^2$ configuration from the parent HS $e_g{}^2t_{2g}{}^3$. We do not provide any spectroscopic nor theoretical evidence for this orbital splitting, but it is noteworthy that this hypothetic model comforts the negative AF Co−O−Co superexchanges within Co_2O_7 dimers (see below). By analogy to $Ca_3Co_2O_6$, another model would consist of a charge-transfer configuration for cobalt. In this compound the prismatic Co^{3+} are possibly assigned to a $Co^{2+}L$ configuration (L = oxygen hole), in better agreement with the calculated charge distribution on Co and on the surrounding oxygen anions.[3] Then, in the title compound, Co^{4+} ($e_g{}^4t_{2g}{}^1$, $S = {}^1/_2$) may correspond to $Co^{3+}L$ ($e_g{}^4t_{2g}{}^2L$) that would produce a local spin-only moment of 2 μ_B/Co^{4+}, and a covalence-induced spin moment on O(2). However, this hypothesis has been rejected because of the difficulty in interpreting the value of the effective moment.

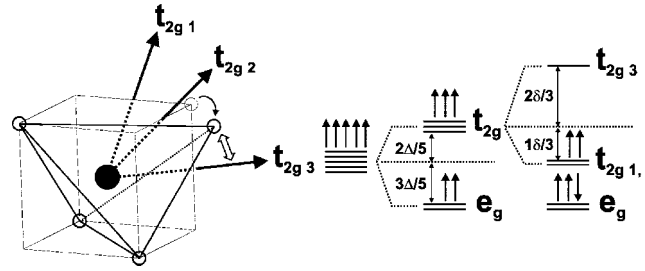

Figure 5. Representation of the t_{2g} orbitals in an tetrahedra and schematization of the resulting orbital diagram.

3.6. Analysis of the Magnetic Exchanges. The local examination of the cation–cation magnetic interaction has been performed step by step, following the cobalt−cobalt interconnection, on the basis of the magnetic susceptibility analysis, the magnetic structure refinement, and the DFT

(24) Radwanski, J.; Ropka, Z. Orbital and Spin Moment in CoO, available online at http://arXiv.org/archive/cond-mat (0310622 V2, publication 11/2003).

(25) Bhide, V. G.; Rajoria, D. S.; Rama Rao, G.; Rao, C. N. R. *Phys. Rev. B: Condens. Matter Mater. Phys.* **1972**, *6*, 1021.

(26) Senaris-Rodriguez, M. A.; Goodenough, J. B. *J. Solid State Chem.* **1995**, *118*, 323.

(27) Kolesnik, S.; Dabrowski, B.; Mais, J.; Majiiga, M.; Chmaissem, O. *Phys. Rev. B: Condens. Matter Mater. Phys.* **2006**, *73*, 214440.

(28) Pouchard, M.; Villesuzanne, A.; Doumerc, J. P. *C. R. Chimie* **2003**, *6*, 135.

calculations. Therefore, octahedral Co^{3+} and tetrahedral IS Co^{4+} should interact as follows.

Tetrameric Units. In $Ba_6Co_6ClO_{15.5}$, the tetrameric Co^{3+} linear units aligned along the *c* axis are reminiscent of the parent 1D 2H-$BaCoO_3$. From the magnetic point of view, it is well-known that linear −M−M− oligomers of this kind, which range from the dimeric units until infinite chains, mostly provide antiferromagnetic (AF) intracouplings largely studied in the field of low-dimensional quantum systems.[29] Thus, face-sharing octahedral blocks show a competition of direct metal−metal exchanges through σ-e'_g and π-a_{1g} overlapping and ∼90° M−O−M superexchanges. The former generally largely predominates as illustrated by the recently described case of $Sr_{1+x}(Cu_xMn_{1-x})O_3$. In this compound, tri- and dimeric units of Mn^{4+} isolated by prismatic Cu^{2+} alternate along the chain axis.[30] For face-sharing octahedral Mn^{4+} ($t_{2g}^3e_g^0$), the Kanamori−Goodenough rules[31] indicate ferromagnetic (F) exchanges for the three possible Mn^{4+}−O−Mn^{4+} superexchanges types (delocalization e_g-p-t_{2g}, correlation e_g−p−t_{2g} and correlation e_g−pσ−pσ'−e_g). However, the susceptibility measurements have shown strong AF couplings well-reproduced by AF Heisenberg–Dirac Van Vleck-like units. It is due to strong AF Mn^{4+}−Mn^{4+} couplings expected for direct exchanges between filled and half-filled d orbitals [d(Mn−Mn) ∼ 2.56 Å]. In the case of half-filled (HS Co^{3+}) and filled orbitals (LS Co^{3+}), the direct t_{2g}−t_{2g} coupling is virtual because LS Co^{3+} does not have a magnetic moment, and then the direct magnetic exchange is realized by correlation transfer from LS to HS cations. It is predicted to be positive (F) with respect to the conservation of the spin between the two magnetic centers. This comforts the DFT calculations for the title compound that predicts strong F couplings within the tetramers but associated with small localized moments. Furthermore, this aspect is reinforced by the shorter Co−Co separations of ∼2.45 Å. The spin-scattering reduction within these units will be discussed later in our work.

Co^{4+} Dimers. Figure 6a shows the different types of d_{Co}−p_O−d_{Co} magnetic interactions within the $Co^{4+}{}_{tetra}$−$Co^{4+}{}_{tetra}$ clusters. The spatial extension of the tetrahedral d orbitals combined to wave functions symmetries do not allow the overlapping between e_g metal orbitals and the oxygen p_σ nor p_π orbitals. Then, as shown in Figure 6a, within the corner sharing tetrahedral [Co(3)−O(4)−Co(3) = 152°] t_{2g}−p_σ−t_{2g} superexchanges drive the nature of the coupling sign. According to Kanamori−Goodenough rules, the proposed mechanisms illustrated in Figure 6a for tetrahedral IS Co^{4+} cations predict antiferromagnetic exchanges for both the correlation and delocalization interactions, in good agreement with neutron diffraction experiments and DFT calculations. It is noteworthy that for symmetrical reasons the three t_{2g} orbitals are equally concerned in the electronic transfer if the oxygen apex was centered on its special position. Then, the off-centring of the O(4) corner probably

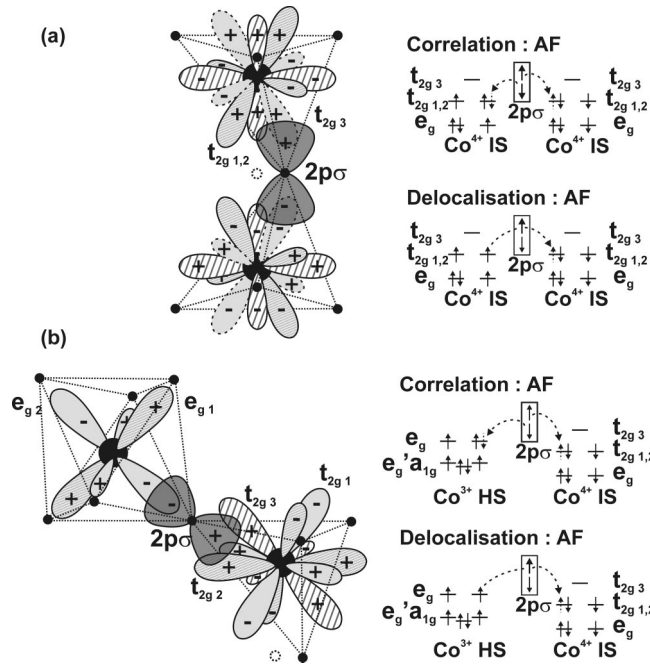

Figure 6. d_{Co}−p_O−d_{Co} magnetic interactions for (a) the $Co^{4+}{}_{tetra}$−$Co^{4+}{}_{tetra}$ and (b) the $Co^{3+}{}_{octa}$−$Co^{4+}{}_{tetra}$ isolated clusters.

stabilizes the system via a maximal overlapping of its involved p orbital with the empty t_{2g} orbital, while the overlapping with the two remaining half-filled t_{2g} is reduced. It may be argued that the repelling of O(4) outside its normal position is caused by the creation of a Co−Co bonding, but the Co−Co separation of 3.510(1) Å appears unlikely for this. It is also worth remembering that in the case of compounds with similar but disconnected blocks, such as $Ba_6Co_5BrO_{14}$ and $Ba_7Co_6BrO_{16.5}$,[14] same splitting of one tetrahedral apex is observed without any possible Co−Co bonding. This scheme is a complementary picture of the energy level splitting of the t_{2g} manifold shown in Figure 5.

Octahedral−Tetrahedral Junction. Figure 6b shows the orbital diagram at the $Co^{3+}{}_{octa}$−$Co^{4+}{}_{tetra}$ interface. Here, the octahedral t_{2g} manifold consists of a singlet a_{1g} and a doublet e'_g favored by the trigonal distortion, with the former being directly oriented along the *c* axis and responsible for possible metal−metal bondings. The rather low splitting has not been highlighted on Figure 6b. It is rather ambitious to analyze this exchange on the basis of the spin configurations deduced from the paramagnetic regime, because below T_N no local ordered moments have been deduced. However, on this basis, only the t_{2g}−p_σ−e_g superexchanges are viewable between HS $Co^{3+}{}_{octa}$ and IS $Co^{4+}{}_{tetra}$ under the M−O−M 180° approximation [Co(1)−O(2)−Co(3) = 164°] (Figure 6b). The correlation and delocalization mechanisms between octahedral HS Co^{3+} and tetrahedral IS Co^{4+} give rise to negative exchanges. Contrarily, according to the experiment and DFT calculations, the competition between them is largely in favor of ferromagnetic correlation. One should also recall that hypothetical AF octa−tetra interactions at both sides of ferromagnetic tetramers would lead to the unobserved doubling of the magnetic cell. Then, ferromagnetic Co^{3+}−O−Co^{4+} Zener's double exchange is plausible.[32] It is also likely that the magnetic contribution ∼0.3 μB

(29) Whangbo, M. H.; Koo, H. J.; Dai, D. *J. Solid State Chem.* **2003**, *176*, 417.
(30) El Abed, A.; Gaudin, E.; zur Loye, H.-C.; Darriet, J. *Solid State Sci.* **2003**, *5*, 59.
(31) Goodenough, J. B. *Magnetism and the Chemical Bond*; Wiley-Intersciences: New York, 1963.

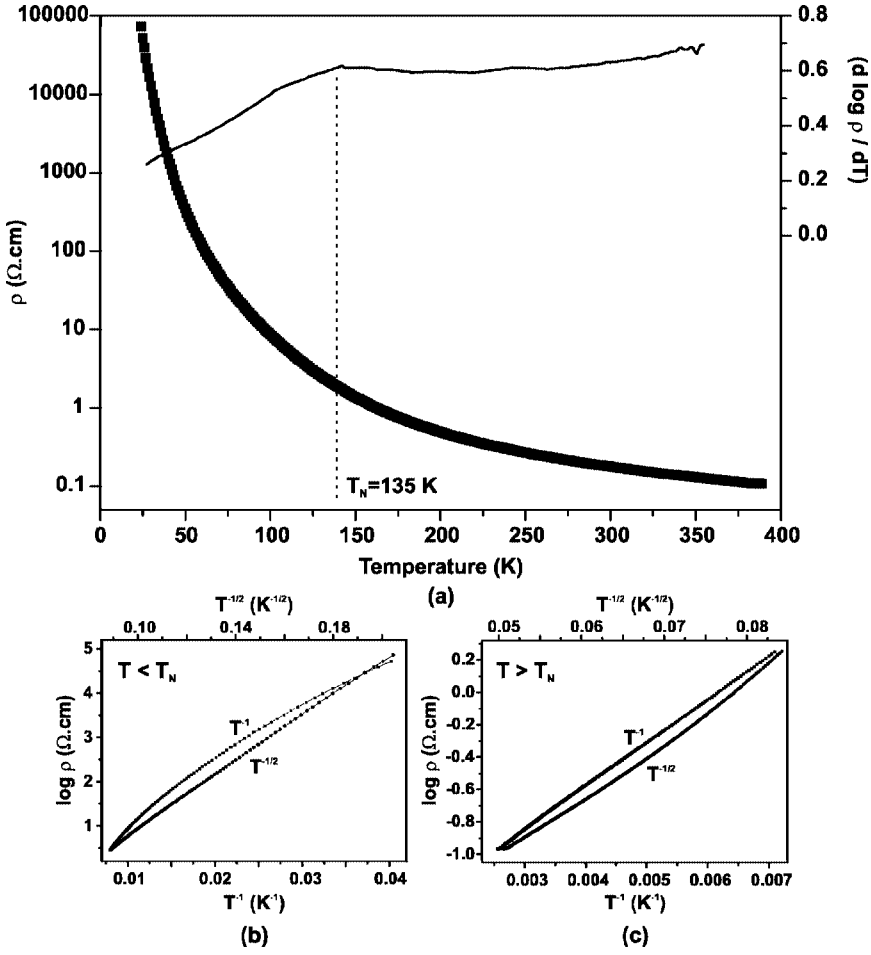

Figure 7. (a) Temperature dependence of the resistivity for the $Ba_6Co_6ClO_{15.5}$ compound. The temperature dependence on different powers (T^{-1} and $T^{-1/2}$) of log ρ are also plot (b) below and (c) above $T_N = 135$ K.

calculated by DFT on the shared O(2) atom is likely mediating the Co−Co exchange in a ferromagnetic way.

3.7. Electric Properties. Figure 7a presents the $Ba_6Co_6ClO_{15.5}$ resistivity thermal evolution. A semiconducting behavior is observed from 400 K to low temperature. The resistivity values at 400 K are $\rho \sim 0.1$ Ω cm for 6H-$Ba_6Co_6ClO_{15.5}$ and 2H-$BaCoO_3$ and $\rho \sim 1$ Ω cm for 12H-$Ba_{0.9}CoO_{2.6}$. From the structural point of view, the title compound 6H-$Ba_6Co_6ClO_{15.5}$ can be derived from 2H-$BaCoO_3$ by introducing cubic layers in the hexagonal matrix; therefore, breaking the 1D columns of face-shared octahedra to a 3D interconnection of Co^{4+} dimers and Co^{3+} tetramers. In both the 5H and 12H $BaCoO_{3-\delta}$ derivatives, the chains are disconnected, in good agreement with the greater experimental resistivity. Then, the creation of several disconnection points that can be seen as disordered centers able to scatter the mobile electrons is an efficient way to create an Anderson localized system for a low-dimension system (from an electric transport point of view), leading to a poor conductivity.[8] This same "localized" origin is at the basis of early explanations for the structurally 1D $BaCoO_3$ associated with a variable range hoping (VRH) of the conductivity and thermoelectric power.[7,33] In $Ba_6Co_6ClO_{15.5}$ from room temperature to $\sim T_N$, the resistivity is characteristic of a semiconductor with a low gap, $\Delta = 0.053$ eV, according to the good linearity of the Arrhenius plot, $\rho = A \exp(-\Delta/(kT))$ (Figure 7c). At high temperature, log ρ versus $T^{-1/2}$ does not match a linear law and an efficient "in plane" electronic conductivity is expected. Below 100 K, a change in the conductivity regime is evidence on d(log ρ)/d(T) versus T plot, while the temperature dependence of ρ becomes more pronounced. Then, the analysis of the temperature dependence of log ρ for T^{-1} and $T^{-1/2}$ shows a linear behavior for the former (Figure 7b), characteristic of a 1D localized system (as in the 2H-$BaCoO_3$), confirming the preferential conductivity along the c-axis polyhedra chains. It is typical of VRH and can be observed for 1D hopping between localized states (Anderson localization) or in the case of a coulomb gap with strong e−e interactions independent of the dimensionality of the system (Efros−Shklovskii model).[34] *A priori*, the ES mechanism can not be excluded from the data. Nevertheless, because our sample should exhibit a preferential conductivity along the c axis, the 1D hopping appears more plausible. Especially, below T_N, most of the sites (Co^{4+}) of the (a and b) conduction paths are antiferromagnetically aligned, which leads to strong constraints for the carriers. Nevertheless, one should keep in mind that our

(32) Zener, C. *Phys. Rev.* **1951**, *81*, 440.
(33) Felser, C.; Yamaura, K.; Cava, R. J. *J. Solid State Chem.* **1999**, *146*, 411.
(34) Efros, A. L.; Shklovskii, B. I. *J. Phys. C: Solid State Phys.* **1975**, *8*, L49.

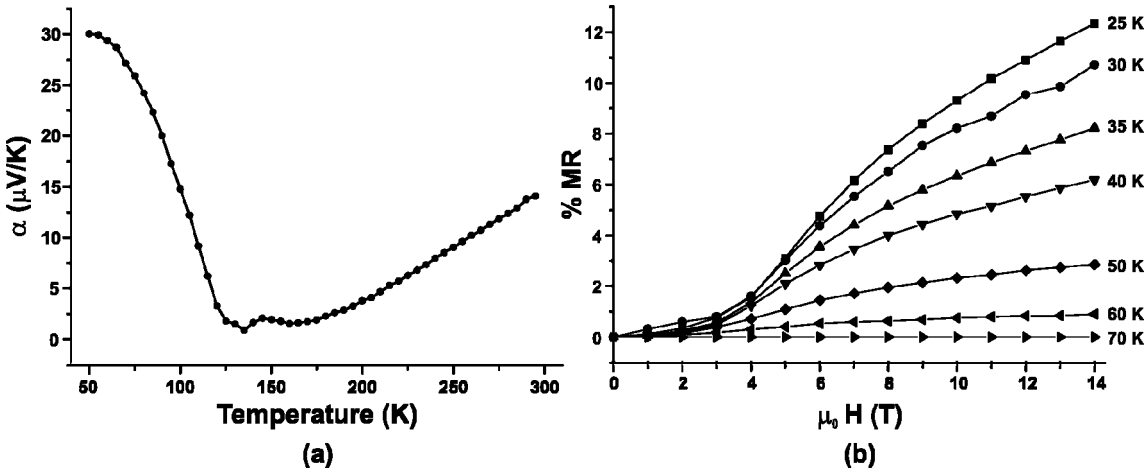

Figure 8. For $Ba_6Co_6ClO_{15.5}$, (a) dependence of the thermoelectric Seebeck coefficient on temperature and (b) isothermal magnetic field-dependent magnetoresistance.

sample is a powder and that the statistical averaging process/grain boundaries effects can attenuate this 1D character.

The temperature dependence of the thermoelectric Seebeck coefficient of $Ba_6Co_6ClO_{16}$ compound at zero field is presented on Figure 8a. The Seebeck coefficient is small and positive over the measured temperature range, indicating that the transport is dominated by *p*-type carriers (holes). This first result agrees well with the mean +3.33 valence in the conduction that arises from the transfer of extra hole carriers (Co^{4+}) to negative acceptors (Co^{3+}). From 300 to 140 K, the Seebeck coefficient slowly decreases to reach a value approximately equal to zero at 135 K. This comforts the thermally activated mobility of preponderant p carriers with respect to the specificity of each Co site. Theoretically, at $\alpha \sim 0$, the hole mobility is caught up by electron motion in an unfavorable ratio for conduction. The increasing of $\alpha(T)$ below $T_N = 135$ K, as the temperature further decreases, denotes the similar progressive but rapid change setting of the magnetic order that modifies the spin degeneracy contribution of the Seebeck coefficient, as already reported in numerous cases.[35] However, the value of α is very small, considering the large resistivity of the material. Only few results concerning the Seebeck coefficients of these 1D materials can be found. It has been shown that α is positive in $Ba_5Co_5ClO_{13}$, with $\alpha \sim +500$ μV/K at 175 K, with this large value being in good agreement with the large resistivity measured in these crystals (with an activation energy $E_g = 0.25$ eV).[11] On the other hand, α is almost zero in $BaCo_2O_4$, in which Co is present only in tetrahedral sites, even if the resistivity is large and semiconductor-like.[36] This small thermopower was ascribed to a possible hybridization of the metallic states with the oxygen band. In $Ba_6Co_6ClO_{15.5}$, such a phenomenon leading to a smaller thermopower could also occur, considering the possibility of itinerant magnetism arising from the direct exchange mechanism in tetramers.

Figure 8b shows the isothermal field-dependent magnetoresistance (MR) curves, in which the MR is defined as % $MR = 100((\rho_H - \rho_{H=0})/\rho_H)$. The magnetoresistance is positive because ρ gradually increases as the temperature decreases below 70 K. It reaches a value of 12% at 25 K and 14 T. Then, the negative term generally observed in magnetic oxides is not apparent. Because of the presence of numerous grain boundaries in our sample, it is hazardous to try a quantitative analysis of the MR effect. Nevertheless, one can note that (i) the MR magnitude increases when the temperature decreases and (ii) the MR can be well-described by the functional form $\ln(\rho_H/\rho_{H=0}) \alpha H^n$, with $n = 2$ in the low field and showing a tendency toward saturation at the high field. These two points can be classically expected in VRH or ES systems because of the shrinkage of the wave function,[37] but as already developed in the electric section, the former is more plausible.

3.8. Tetrameric Units as Traps for Electrons. One could not properly describe our system without any mention on the apparent drastic spin-scattering reduction below T_N assigned to the tetrameric Co(1) and Co(2). Above T_N, the value of the effective moment indicates that the terminal Co(1) are likely associated to a HS Co^{3+} state ($S = 2$), while Co(2) is LS ($S = 0$). However, below T_N, both ND data and DFT calculations indicate rather important changes highlighted by the weak value of the localized moments for both sites. This feature is particular by a comparison to what is going on in the related $BaCoO_{3-\delta}$ phases. The $\delta = 0$ is particular because we are dealing with LS Co^{4+} ($S = {}^1/_2$) and there is no clear consensus about its ground state that is experimentally evidenced as a weak ferromagnetic likely arising from AF exchanges between 1D ferromagnetic chains. Furthermore, no ND data are available at that time. However, LDA + U calculations have shown, whatever the magnetic structure is, non-negligible moments (0.65–0.90 μB/Co) inside each Co sphere, with the rest of the magnetic moment lying inside the O spheres and the interstitial region.[4] Closer to the title compound, the 5H and 12H forms of $BaCo_{3-\delta}$ contain tri- and tetramers similar to the tetrameric units of $Ba_6Co_6ClO_{15.5}$, mainly occupied by Co^{3+} species. For both compounds, ferromagnetic orderings have been evidenced

(35) Mentré, O.; Dhaussy, A. C.; Abraham, F.; Steinfink, H. *J. Solid State Chem.* **1997**, *130*, 223.
(36) Boulahya, K.; Parras, M.; Gonza, J. M.; Amador, U.; Marti, J. L.; Ferna, M. T. *Chem. Mater.* **2006**, *18* (16), 3898.
(37) Shklovskii, B. I.; Efros, A. L. *Electronic Properties of Doped Semiconductors*; Springer: Berlin, Germany, 1984.

and ND data indicate localized magnetic moments of ~3.5 and ~1 μB on the octahedral cobalt at low temperature.

In the title compound, neglecting the spin–orbit interaction, it appears clearly that the tetrahedral Co^{4+} nearly conserve their account of electron below T_N ($S_{paramagn} = {}^3/_2$ and $m_{4K} = 2.8$ μB), while the two octahedral Co^{3+} behave similarly ($S_{paramagn} = 2$ and 0 and $m_{4K} = 0.5$ and 0.6 μB). It is worth stating again that their refined moments can vary from 0 to 0.8 μB without drastic change in the quality of the refinement, therefore suggesting a probable strong itinerant delocalization confined in the tetrameric units. In addition, the magnetic moments are likely diluted toward the surrounding oxygen, but one should keep in mind that tetramers behave as forceful ferromagnetic connectors between strong AF Co^{4+} dimers. Then, below T_N, they can be qualitatively considered as insulating fences mainly responsible for the resistivity increase and the VRH regime. A good clue for this is the strong hybridization of Co(3) with O(2), at the tetrahedral−octahedral junction and the 0.3 μB located on this common oxygen calculated by DFT.[16] The mechanism for the magnetic transmission within the tetrameric units has been proposed above. To explain the observed vanishing of local moments in these entities, we could add that, because of the formal LS state for Co(2), Co(1)−O−Co(2) and Co(2)−O−Co(2) superexchanges with angles of about 80° have not been considered but have been shown to be responsible for the intrachain ferromagnetism through an orbital ordering in $BaCoO_3$.[4] As a matter of fact, our previous DFT calculation showed no residual magnetic moment on the oxygen of the chains in the oxychloride. Hence, the electronic transfer/correlation is likely affected by direct Co−Co exchanges [d(Co−Co) ~ 2.48 Å]. Band structure calculation study on $BaCoO_3$ has suggested that it is mediated[33] by π bonding between d_{zx} and d_{yz} orbitals. Of course, σ overlapping between t_{2g} orbitals is also possible with contact angles of ~120°. Then, part of the electrons could be considered as delocalized along these paths, while an important amount should also be engaged in the partially covalent Co−O bonds.

4. Conclusion

We have shown here the possibility to describe most of the magnetic phenomena occurring in the mixed valence compound $Ba_6Co^{3+,4+}{}_6ClO_{15.5}$ on the basis of relatively simple models, such as superexchanges and double exchanges mediated by orbital overlapping. This analysis has been effected step by step in the different subunits of the crystal lattice. A good correlation between magnetic and transport properties has been pointed out through the analysis of resistivity and Seebeck coefficients changes below T_N = 135 K. In this domain, a VRH regime is obtained, assigned to possible Anderson-like localization, and below 70 K, magnetoresistance has been detected. However, the most exciting result concerns what is going on in isolated Co_4O_{15} terameric units of face-sharing octahedral, in which the ordered magnetic moments appear null by neutron diffraction, while magnetic susceptibility assess a mixture of HS and LS Co^{3+}. This spin-scattering reduction associated with the insulating regime below T_N is in favor of a magnetic dilution toward the bridging oxygen and in the intermediate M−M region. The resulting groups act as strong ferromagnetic connectors between terminal tetrahedral Co^{4+} cations.

Acknowledgment. The Institut Laue Langevin (Grenoble, France) is thanked for providing neutron facilities, and Dr. Emmanuelle Suard is gratefully acknowledged for her help in the data collection. The authors are very grateful to Dr. Vaclav Petricek (Academy of Sciences, Czech Republic) for providing them the beta version of JANA2006, allowing thus the combined refinement presented in the manuscript. The "Fonds Européen de Développement Régional" (FEDER), "Centre National de la Recherche Scientifique" (CNRS), "Région Nord Pas-de-Calais", and the "Ministère de l'Education Nationale, de l'Enseignement Supérieur et de la Recherche" are acknowledged for funding of X-ray diffractometers. M.K. is also grateful to the CNRS and the Région Nord Pas-de-Calais for the funding of his Ph.D. grant. Finally, the authors are very grateful to Prof. Francis Abraham (UCCS Lille, France) for fruitful discussion.

Supporting Information Available: Atomic coordinates and anisotropic displacement parameters for $Ba_6Co_6ClO_{15.5}$ at room temperature, resulting from a combined refinement with neutron powder (λ = 1.594 Aring), X-ray powder ($\lambda K_{\alpha 1\text{-}Cu}$ = 1.54056 Aring), and X-ray single-crystal data ($\lambda K_{\alpha\text{-}Mo}$ = 0.71073 Aring), conducted using the beta version of JANA2006. This material is available free of charge via the Internet at http://pubs.acs.org.

CM702678V